Croatian Society for Materials Protection

Metalurgija/Metallurgy

Vol. 65 No. 4 / 2026

Research on Performance Improvement Strategies for Clothing Zippers in High Wear and Corrosion Environments

Ruoyan Ning [1] and Tianjiao Zhang [2,*]

https://doi.org/10.64486/m.65.4.14

[1] Zhejiang Sci-Tech University, Linping District, Hangzhou 311106, Zhejiang, China
19012728613@163.com
[2] Harbin Vocational College of Science and Technology, Harbin City, Heilongjiang Province, China
19845181007@163.com
* Correspondence: 19845181007@163.com

Type of the Paper: Article
Received: January 6, 2026
Accepted: April 29, 2026.

Abstract: With the rapid development of outdoor sports, marine operations, and special work clothing, the performance failure of clothing zippers in high wear-corrosion coupling environments has become increasingly prominent. Traditional metal zippers have low surface hardness and insufficient corrosion resistance, making it difficult to meet the long-term use requirements under complex working conditions. This paper proposes a surface engineering strategy based on laser cladding technology, which in-situ prepares a Stellite 12 cobalt-based alloy coating on the surface of 304 stainless steel zipper teeth. The microstructure, wear resistance, and corrosion resistance of the coating are systematically studied. The results show that the laser cladding coating forms a metallurgical bond with the substrate, forming a composite structure of "γ-Co solid solution matrix + hard carbide eutectic". The microhardness of the coating is significantly improved; friction and wear tests show that its wear loss is greatly reduced compared with the substrate, and the corrosion current density decreases by an order of magnitude in the corrosive environment, demonstrating excellent comprehensive performance. This study provides a feasible material and process solution for improving the service performance of zippers in harsh environments, and has important theoretical value and practical significance for promoting the development of high-end functional clothing.

Keywords: clothing zippers; laser cladding; wear resistance; corrosion resistance

1. Introduction

Clothing zippers, as indispensable functional components of modern clothing, have performance reliability that serves as one of the key indicators for evaluating the overall quality of clothing. With the rapid development of outdoor sports, marine operations, and special industries, the service environment of clothing zippers has become increasingly harsh, exposing them to long-term high-wear and high-corrosion coupling working conditions. Frequent mechanical friction between zipper teeth and sliders, combined with chemical corrosion from media such as sweat and salt spray, easily leads to zipper jamming, cracking, or surface corrosion, thereby causing functional failure.

The core of this problem lies in the insufficient surface performance of traditional metal zipper materials. Although 304 austenitic stainless steel is widely used due to its good corrosion resistance [1], its low surface hardness (about 200 HV) makes it difficult to resist severe wear; meanwhile, its relatively poor impact toughness and short service life (caused by cyclic loading) are inherent flaws. Therefore, developing a new technology that can simultaneously endow zipper substrates with ultra-high hardness, excellent wear resistance, and outstanding corrosion resistance has become an urgent research topic in the clothing accessory field with significant engineering value.

Surface engineering is an effective approach to enhance material surface performance and extend component service life. Among various surface technologies, laser cladding technology exhibits unique advantages [2]. This technology fuses alloy powder and the substrate surface synchronously through a high-energy laser beam, followed by rapid cooling, enabling the preparation of functional coatings with precisely designed composition and structure [3]. It can easily control the shape, thickness, composition, and microstructure of the coating [4].

Currently, laser cladding has been successfully applied to the strengthening and repair of key components in aerospace, energy, and other fields, demonstrating great potential in improving the extreme performance of material surfaces [5-6]. However, systematic research on applying this technology to small-sized, precision-structured consumer goods (e.g., clothing zipper teeth) is still in its infancy, especially lacking in-depth work on systematically explaining coating construction mechanisms and their influence laws on core zipper performance from the perspective of surface engineering.

Based on this, this study innovatively proposes laser cladding technology as a surface engineering strategy, in-situ preparing a cobalt-based superalloy (Stellite 12) coating on 304 stainless steel zipper teeth surfaces to construct a composite system of "tough substrate + ultra-hard surface", aiming to simultaneously overcome the bottlenecks of wear and corrosion resistance. Stellite 12 alloy, rich in elements such as Cr and W, combines excellent wear resistance, corrosion resistance, and certain toughness, making it an ideal surface strengthening material [7-9]. By achieving metallurgical bonding between this alloy and 304 stainless steel substrates via laser cladding, it is expected to significantly improve the surface performance of zippers while retaining the overall performance of the substrate.

The research framework of this paper is as follows: First, optimize the laser cladding process to realize high-quality and controllable coating preparation; second, use modern analysis methods to characterize the microstructure, phase composition, and interface properties of the coating; then, comprehensively evaluate the wear resistance of the coating and its electrochemical behavior in simulated corrosion environments, revealing the micro-mechanism of performance improvement. This study aims to establish a surface functionalization method suitable for micro metal products such as clothing zippers, providing new technical ideas and theoretical support for the development of high-end functional clothing.

2. Experimental Methods

Commercial cold-rolled 304 austenitic stainless steel was selected as the substrate material, with its chemical composition listed in Table 1. The substrate was processed into 15 mm × 15 mm × 5 mm samples to simulate individual zipper teeth. All sample surfaces were ground and polished to a mirror finish, then ultrasonically cleaned with acetone to remove oil stains.

The coating material used was spherical Stellite 12 cobalt-based alloy powder prepared by gas atomization. This powder has high sphericity and good fluidity, and its chemical composition is also listed in Table 1. The particle size range of the powder is (45–105) μm.

Coating preparation was carried out using an LDF 3000-60 fiber laser, equipped with a coaxial powder feeding system and a high-precision mechanical arm [10]. Under an argon protective atmosphere, laser cladding was performed on the substrate surface via synchronous powder feeding. With the goal of obtaining coatings with good metallurgical bonding and no macro defects, the final optimized process parameter combination was determined through systematic optimization of single-pass and multi-pass overlapping processes, as shown in Table 2.

https://doi.org/10.64486/m.65.4.14

Table 1. Chemical Compositions of Substrate and Coating Powder (Mass Fraction/%)

Element	304 Stainless Steel Substrate	Stellite 12 Alloy Powder
C	0.08	1.37
Si	0.77	1.32
Mn	1.60	0.07
Cr	18.04	30.11
Ni	8.04	2.21
W	-	8.11
Co	-	Bal.
Fe	Bal.	2.28

Table 2. Optimized Process Parameters for Preparing Stellite 12 Coating by Laser Cladding

Parameter	Symbol	Unit	Optimized Value
Laser Power	P	W	1400
Scanning Speed	V	mm/s	15
Spot Diameter	D	mm	3
Powder Feeding Rate	F	r/min	1.0
Overlap Rate	η	%	50
Shielding Gas	-	-	High-purity Argon

3. Coating Microstructure and Formation Mechanism

The final performance of the laser cladding coating is determined by its microstructure, which is directly controlled by the thermodynamic and kinetic conditions during the cladding process [11-12]. This chapter systematically characterizes the macroscopic formation, interface bonding characteristics, microstructural morphology, and phase composition of the coating, and deeply analyzes its formation mechanism.

3.1 Macroscopic Formation and Interface Metallurgical Bonding

The Stellite 12 coating prepared with optimized process parameters exhibits good macroscopic formability. The macroscopic morphology of the coating surface is shown in Figure 1: the surface is smooth and continuous, showing a typical laser rapid solidification morphology, with no visible macro defects such as cracks or pores. This indicates that the process parameters are well-matched and the cladding process is stable [13].

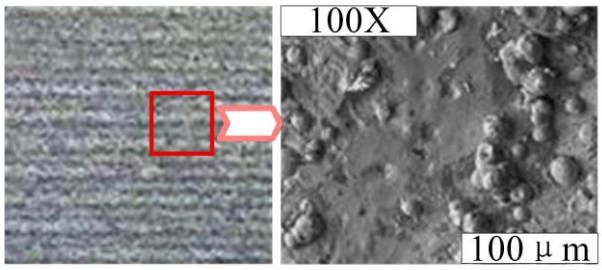

Figure 1. Macroscopic Morphology of Coating Surface [15]

The macroscopic morphology of the coating cross-section is shown in Figure 2. A flat and clear interface is formed between the coating and the 304 stainless steel substrate, with an average coating thickness of approximately 450 μm. Under high magnification, a narrow transition zone (with distinct microstructure different from both sides) can be observed in the interface area. No defects such as cracks or incomplete fusion are found in this zone, confirming the formation of a complete metallurgical bond. The microstructure near the interface shows a transition from planar crystals (on the substrate side) to dendrites (on the coating side), which is determined by the extremely high temperature gradient (G) and relatively fast solidification rate (R) at the bottom of the molten pool [14-15].

https://doi.org/10.64486/m.65.4.14

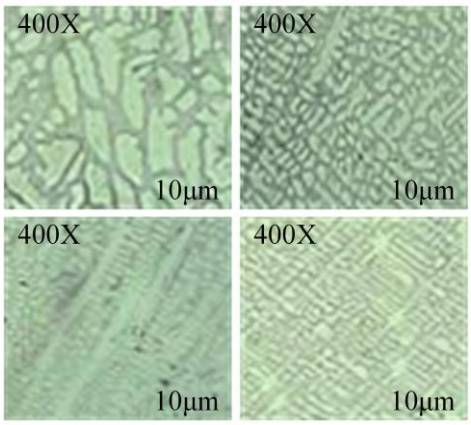

Figure 2. Macroscopic Morphology of Coating Cross-section [9]

To quantitatively evaluate the interface bonding quality, element interaction, and bonding mechanism, EDS line scan analysis was performed on the interface area. The results indicate that the concentrations of main elements (Fe as the substrate characteristic element, Co and Cr as the coating characteristic elements) undergo continuous and steep gradient changes within ~20 μm across the interface, forming an obvious element mutual diffusion zone [8-9]. Based on the Fe content in the coating, the dilution rate of the coating is calculated to be approximately 16.9 %, and this moderate dilution rate has dual significance:

1) It ensures the actual composition of the coating does not deviate excessively from that of Stellite 12 alloy, maintaining its expected excellent performance;
2) It enables metallurgical bonding between the coating and substrate via composition gradient, which coordinates thermal physical parameter differences (e.g., thermal expansion coefficient, elastic modulus) and effectively mitigates interfacial stress—this is the key to the coating system having high bonding strength and long-term service stability.

3.2 Microstructural Morphology and Element Distribution

The typical dendritic microstructural morphology of the coating is shown in Figure 3. The morphology of the interdendritic eutectic structure under backscattered electron (BSE) mode is presented in Figure 4: due to the atomic number contrast effect, there is a significant contrast difference between the dendrite trunk (primary phase) and the interdendritic region—the dendrite trunk shows darker contrast, while the interdendritic region shows brighter contrast. This indicates that the interdendritic region is enriched with heavy elements with higher atomic numbers [16].

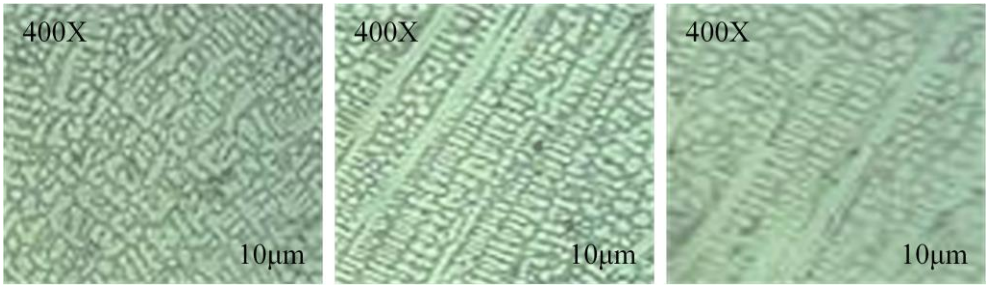

Figure 3. Typical Dendritic Microstructural Morphology of the Coating

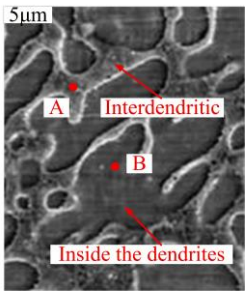

Figure 4. Morphology of Interdendritic Eutectic Structure Under BSE Mode (labeled: A = Interdendrite; B = Inside the dendrites) [17]

https://doi.org/10.64486/m.65.4.14

To clarify the composition of each region, EDS point analysis was performed on the marked points in Figure 4, and the results are listed in Table 3. The analysis shows that the dark-contrast dendrite trunk region is mainly rich in Co, Cr, and W (with low C content), while the bright-contrast interdendritic region is rich in Cr, W, and C.

It can thus be inferred that:

1) The dendrite trunk is primarily a γ-Co solid solution (face-centered cubic structure) formed by the solid solution of elements such as Co, Cr, and W.
2) The interdendritic region is an eutectic structure composed of Cr- and W-rich carbides (e.g., M_7C_3 type) and γ-Co.

This composite structure (a "tough solid solution matrix + hard carbide eutectic network") is the key to the coating achieving a balance between high hardness and good toughness [17].

Table 3. EDS Composition Analysis of Typical Microregions in the Coating (Atomic Fraction/%)

Analysis Position	C	Cr	Fe	Co	W	Inferred Main Phase Composition
Point B	6.59	35.59	2.18	42.59	10.21	γ -Co + $(Cr, W)_7C_3$ eutectic
Point A	3.02	25.38	3.04	58.44	6.57	γ -Co solid solution

3.3 Phase Composition and Formation Mechanism Analysis

The X-ray diffraction (XRD) pattern of the coating is shown in Figure 5. The main diffraction peaks perfectly match the standard card (PDF#15-0806) of γ-Co with a face-centered cubic (FCC) structure, and the diffraction intensity is significantly higher, indicating that γ-Co is the dominant phase in the coating. The extremely high cooling rate of laser cladding (>10^4 K/s) strongly inhibits the phase transformation of γ-Co to the thermodynamically more stable ε-Co (hexagonal close-packed structure), resulting in an extremely low content of ε-Co in the coating—its diffraction peaks (labeled 2 in Figure 5) are very weak, with a calculated volume fraction of less than 3 % based on the relative intensity of diffraction peaks. This low content of ε-Co is of great significance for the coating's performance: ε-Co has higher hardness but poorer toughness compared to γ-Co, and the inhibition of its formation avoids the reduction of coating toughness caused by excessive ε-Co, ensuring the balance between the hardness of the coating (endowed by carbides) and the toughness of the matrix (provided by γ-Co).

In addition, weak diffraction peaks are observed at 2θ° ≈ 44°, 51°, and 75°, which are calibrated to correspond to Cr_7C_3-type carbides [9]. This verifies the inference from EDS that carbides exist in the interdendritic region.

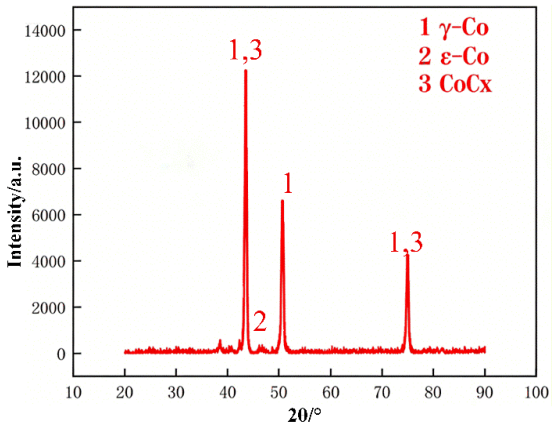

Figure 5. X-ray Diffraction Pattern of the Coating (1 = γ-Co; 2 = ε-Co; 3 = Co_xC_γ)

https://doi.org/10.64486/m.65.4.14

4. Wear and Corrosion Resistance of the Coating

4.1 Wear Resistance

The friction and wear test results are shown in Figure 6. Under dry sliding friction conditions with different loads (10 N, 30 N, 90 N, 150 N), the Stellite 12 coating exhibits better tribological performance than the 304 stainless steel substrate. Error bars in Figure 6 represent the standard deviation (SD) calculated from three repeated measurements (n = 3). To provide a clearer quantitative summary, Table 4 lists the average friction coefficients and their standard deviations for each load condition.

The average friction coefficient of the coating shows a non-linear dependence on load: it decreases at lower loads (10–30 N) and increases at higher loads (90 N–150 N). At 10 N and 30 N, the values are approximately 0.426 and 0.336, respectively, indicating relatively low friction under lower loads. However, as the load increases to 90 N and 150 N, the friction coefficient rises to 0.355 and 0.495, respectively, showing a clear increasing trend under higher loads.

Table 4. Average friction coefficient of Stellite 12 coating under different loads (mean ± SD, n = 3)

Load / N	Average Friction Coefficient (COF)
10	0.426 ± 0.015
30	0.336 ± 0.012
90	0.355 ± 0.010
150	0.495 ± 0.009

Note: The SD values are calculated from three independent repeated tests (n = 3).

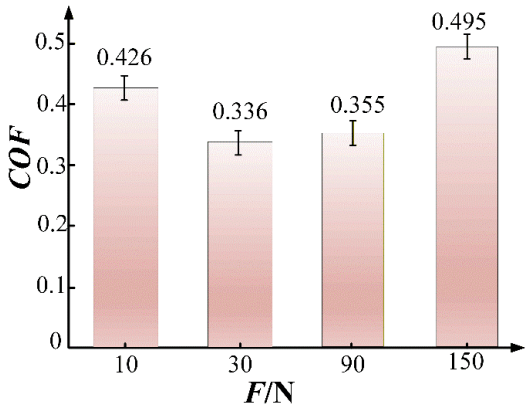

Figure 6. Friction coefficients under different loads (*COF* = Coefficient of Friction; *F* = Load; Error bars represent standard deviation (n = 3)).

The quantitative comparison of wear loss further confirms the significant advantages of the coating. As shown in Table 5, under the test condition of 30 N load and fixed sliding time, the mass loss of the Stellite 12 coating is greatly reduced compared with that of the 304 stainless steel substrate. For the substrate, complete wear loss data under 90 N and 150 N loads are not listed, mainly because 304 stainless steel exhibits extremely severe wear under such high-load dry sliding conditions significant plastic deformation, surface spalling, and even local structural failure occur in a short time, making it impossible to obtain accurate and stable mass loss data through conventional weighing methods. This phenomenon itself also indirectly reflects the insufficient wear resistance of the substrate under harsh high-load conditions, while the coating maintains measurable and stable wear behavior even at 150 N, further verifying its superior wear resistance.

The fundamental improvement in the coating's wear resistance stems from its unique metallurgical properties: the composite structure constructed by laser cladding achieves high hardness through hard $(Cr, W)_x C_\gamma$ carbide strengthening phases dispersed in the γ-Co solid solution matrix [18-20]. These carbide phases can effectively inhibit micro-plastic deformation and material removal during friction, thus endowing the coating

https://doi.org/10.64486/m.65.4.14

with excellent wear resistance from the material characteristic perspective—unlike the single solid solution strengthening mechanism relied on by the substrate.

Table 5. Average wear loss (mg) under different loads

Load /N	10	30	90	150
Coating Wear Loss	5.4	14.7	62.9	156.5
Substrate Wear Loss	-	32.5	-	-

4.2 Corrosion Resistance

Electrochemical polarization tests were conducted to systematically evaluate the corrosion behavior of the coating in 3.5 wt.% NaCl solution. The potentiodynamic polarization curves of the Stellite 12 coating and 304 stainless steel substrate are shown in Figure 7. From the curve shape and key parameters, the significant improvement in the coating's corrosion resistance can be clearly observed [21-22]. Compared with the substrate, the anodic polarization curve of the coating shifts to the right overall, indicating that its anodic dissolution process is more strongly inhibited.

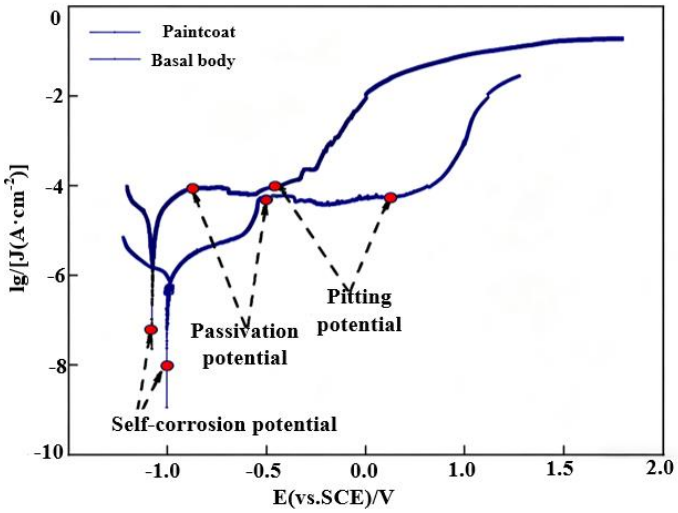

Figure 7. Potentiodynamic Polarization Curves of 304 Stainless Steel Coating and Substrate (Key labels: Passivation potential; Pitting potential; Self-corrosion potential; Curves: Patina coat = Coating; Brass body = Substrate)

Key electrochemical parameters obtained by fitting the polarization curves are listed in Table 6. The self-corrosion potential ($E_{(n)}$) of the coating is -504.5 mV (vs. SCE), which is 75.2 mV positively shifted compared to the substrate (-579.7 mV). This indicates a lower tendency for the coating to undergo corrosion from a thermodynamic perspective. The more critical kinetic parameter—corrosion current density ($i_{(n)}$)—shows that the coating (2.02×10^{-7} A·cm^{-2}) is reduced by an order of magnitude compared to the substrate (4.27×10^{-6} A·cm^{-2}), and the calculated corrosion rate also decreases significantly. This directly confirms that the coating can effectively slow down the corrosion reaction process.

The excellent corrosion resistance of the coating is mainly attributed to its Cr content of up to 30 wt.%, which ensures the rapid formation of a dense and stable Cr_2O_3 passive film in corrosive media, thereby providing effective barrier protection [23-24].

https://doi.org/10.64486/m.65.4.14

Table 6. Electrochemical Corrosion Parameters of Coating and Substrate

Sample	Self-corrosion Potential $E_{(n)}$/(mV vs. SCE)	Corrosion Current Density $i_{(n)}$/(A·cm^{-2})	Calculated Corrosion Rate/(mm/a)
304 Stainless Steel Substrate	-579.5	4.27×10^{-6}	0.0501
Stellite 12 Coating	-504.3	2.02×10^{-7}	0.0025

5. Discussion

This study confirms that constructing a Stellite 12 cobalt-based alloy coating on the surface of 304 stainless steel via laser cladding technology can simultaneously significantly improve its surface wear and corrosion resistance. This breakthrough in comprehensive performance originates from the unique non-equilibrium microstructure formed by laser rapid solidification, and the synergistic effect of the strengthening and passivation mechanisms it brings.

The excellent mechanical properties of the coating stem from its "γ-Co solid solution matrix + hard carbide eutectic" composite structure. At an ultra-high cooling rate (>10^4 K/s), alloy elements (Cr, W) precipitate as (Cr, W)$_x$C$_\gamma$ in the γ-Co solid solution, and a dense (Cr, W)$_x$C$_\gamma$ carbide network is distributed between the dendrite trunks. This structure produces two strengthening effects: grain refinement strengthening and second-phase dispersion strengthening. This directly leads to a leap in the coating's hardness compared to the substrate, fundamentally changing the material's response behavior during friction.

During friction and wear, the high hardness and hard framework of the coating result in only slight abrasive wear (shallow grooves on the surface), while the soft 304 stainless steel substrate undergoes severe plastic deformation and adhesion, showing a combination of abrasive and adhesive wear (deep grooves and spalling on the surface) [7,13,18]. Therefore, the significant improvement in wear resistance is the result of the synergistic effect of the coating's composite structure, which effectively solves the problem of geometric distortion and functional degradation of zippers caused by mechanical wear.

Meanwhile, this non-equilibrium structure also lays the foundation for the substantial improvement in corrosion resistance. The Cr content (up to 30 wt. %) in the coating mainly exists in the uniform γ-Co matrix in solid solution form, rather than concentrating in coarse phases that are prone to localized corrosion. Electrochemical tests show that this homogeneous solid solution structure promotes the rapid formation of a dense and stable Cr_2O_3 passive film on the entire surface, reducing the corrosion current density by an order of magnitude. This uniform passive film provides an effective chemical barrier, significantly inhibiting the occurrence of pitting corrosion, and ensuring the long-term stable service of zippers in corrosive environments such as sweat and salt spray.

In summary, the laser cladding surface engineering strategy adopted in this study has core value in constructing both a "mechanical barrier" and a "chemical barrier" on the material surface through a single process. This non-equilibrium microstructure design based on rapid solidification simultaneously meets two key requirements: "high hardness and hard phase reinforcement" for resisting mechanical damage, and "uniform Cr-rich solid solution" for resisting electrochemical corrosion. This strategy provides an innovative, efficient, and promising material solution for fundamentally solving the wear-corrosion coupling failure problem of clothing zippers in complex service environments.

6. Conclusions

In this study, a Stellite 12 cobalt-based alloy coating was successfully prepared on the surface of 304 stainless steel via laser cladding technology. The microstructure, mechanical properties, and corrosion resistance of the coating were systematically investigated.

The results show that the optimized process enables the coating to form a good metallurgical bond with the substrate, with an obvious element diffusion transition zone at the interface. The coating is mainly

https://doi.org/10.64486/m.65.4.14

composed of a γ-Co solid solution matrix and $(Cr, W)_xC_\gamma$ carbide eutectic distributed in the interdendritic region; this composite structure endows the coating with a balance of high hardness and toughness.

Friction and wear tests indicate that the coating exhibits a more stable low friction coefficient under different loads, and its wear loss is significantly lower than that of the substrate. The improvement in wear resistance mainly originates from the effective load-bearing support and plastic deformation resistance of the hard carbide phases.

Electrochemical tests confirm that in 3.5 wt. % NaCl solution, the coating shows a positive shift in self-corrosion potential and a reduction in corrosion current density by an order of magnitude. This benefit comes from the dense Cr_2O_3 passive film formed due to the high Cr content.

This study verifies that the laser-clad Stellite 12 coating can simultaneously enhance the wear and corrosion resistance of 304 stainless steel. It provides an effective surface engineering solution for the long-term reliable service of clothing zippers in high wear-corrosion coupling environments, and has good application potential.

References

[1] J. R. Davis, Stainless Steels. Materials Park, OH, USA: ASM International, 1994. https://doi.org/10.1361/asmhba0001340

[2] S. Yin, et al. "Hot corrosion behavior of laser cladded (AlTiCrNbTa)O2 high-entropy ceramic coatings in various molten salts." Ceramics International, vol.52, no.4, pp.5156-5173, 2026, https://doi.org/10.1016/J.CERAMINT.2025.12.290

[3] F. Weng, C. Chen, and H. Yu, "Research status of laser cladding on titanium alloys: A review" Materials & Design, vol.58, pp.412-425, 2014, https://doi.org/10.1016/j.matdes.2014.01.077

[4] J. A. Vreeling, V. Ocelík, J. T. M. De Hosson, and Y. T. Pei, "Laser melt injection of WC particles in aluminium alloys" Materials Science and Engineering: A, vol.336, no.1-2, pp.1-8, 2002, https://doi.org/10.1016/S0921-5093(02)00009-7

[5] C. P. Paul, S. H. Alemohammad, E. Toyserkani, and A. Khajepour, "Cladding of WC–12Co on low carbon steel using a pulsed Nd: YAG laser" Materials Science and Engineering: A, vol.464, no.1-2, pp.170-176, 2007, https://doi.org/10.1016/j.msea.2007.02.087

[6] R. L. Sun, Y. W. Lei, and W. Niu, "Laser cladding of Stellite 6 on stainless steel to enhance solid particle erosion and cavitation resistance" Surface and Coatings Technology, vol.204, no.1-2, pp.15-24, 2009, https://doi.org/10.1016/j.surfcoat.2009.06.028

[7] Y. Huang, X. Zeng, Q. Hu, and S. Zhou, "Corrosion behaviour of laser-clad Stellite 6 alloy in simulated body fluid" Corrosion Science, vol.51, no.8, pp.1706-1714, 2009, https://doi.org/10.1016/j.corsci.2009.04.019

[8] C. Navas, A. Conde, B. J. Fernández, F. Zubiri, and J. Damborenea, "Laser coatings to improve wear resistance of mould steel" Surface and Coatings Technology, vol.194, no.1, pp.136-142, 2005, https://doi.org/10.1016/j.surfcoat.2004.07.068

[9] J. H. Abboud, K. Y. Benyounis, and P. H. Shipway, "Microstructure and abrasive wear behaviour of laser clad Stellite 6 alloy" Journal of Materials Processing Technology, vol.206, no.1-3, pp.215-221, 2008, https://doi.org/10.1016/j.jmatprotec.2007.12.046

[10] I. Hemmati, V. Ocelík, and J. T. M. Hosson, "Dilution effects in laser cladding of Ni–Cr–B–Si–C hardfacing alloys" Materials Letters, vol.84, pp.69-72, 2012, https://doi.org/10.1016/j.matlet.2012.06.048

[11] Y. Chen, and H. M. Wang, "Growth characteristics of primary M7C3 carbide in laser clad Fe–Cr–C–Ni–B coating" Materials Science and Engineering: A, Vol.391, no.1-2, pp.324-329, 2004, https://doi.org/10.1016/j.msea.2004.09.010

[12] M. Zhong, W. Liu, and H. Zhang, "Corrosion and wear resistance characteristics of NiCr coating by laser cladding in seawater" Journal of Materials Processing Technology, vol.180, no.1-3, pp.328-335, 2006, https://doi.org/10.1016/j.jmatprotec.2006.07.001

[13] H. T. Jin, F. Y. Luo, and Y. Z. Luo, et al. "Study on wear and corrosion behaviors of nano VC enhanced CoCrNi medium-entropy alloy coatings by laser cladding." Journal of Materials Research and Technology, vol.42, pp.1776-1792, 2026, https://doi.org/10.1016/J.JMRT.2026.03.216

[14] P. Farahmand, and S. Liu, "Laser cladding of Stellite 6 on P91 steel for improved wear and corrosion resistance" Surface and Coatings Technology, vol.206, no.19-20, pp.4252-4260, 2012, https://doi.org/10.1016/j.surfcoat.2012.04.032

https://doi.org/10.64486/m.65.4.14

[15] M. J. Chao, and W. L. Wang, "Erosion–corrosion behaviour of laser-clad Stellite 6 alloy in saline slurry" Wear, vol.260, no.11-12, pp.1348-1353, 2006, https://doi.org/10.1016/j.wear.2005.09.007

[16] V. Ocelík, D. Matthews, and J. T. M. Hosson, "Sliding wear resistance of metal matrix composite layers prepared by laser melt injection" Wear, vol.258, no.1-4, pp.357-364, 2005, https://doi.org/10.1016/j.wear.2004.09.023

[17] X. Wu, and Y. Hong, "Friction and wear behaviour of laser clad TiC–Ni composite coating" Wear, vol.250, no.1-12, pp.1290-1297, 2001, https://doi.org/10.1016/S0043-1648(01)00759-9

[18] Q. Li, D. Zhang, T. Lei, C. Chen, and W. Chen, "Comparison of laser-clad and furnace-melted Ni-based alloy microstructures" Surface and Coatings Technology, vol.202, no.14, pp.3360-3366, 2008, https://doi.org/10.1016/j.surfcoat.2007.12.007

[19] Y. L. Gao, S. Jiang, and Y. Liu et al. "Microstructure Characteristic and Wear Resistance of Al2CrFeNiMoSix High-Entropy Alloy Coating on Cr12MoV by Laser Cladding." Journal of Thermal Spray Technology, pp.1-16, 2026, https://doi.org/10.1007/S11666-026-02185-7

[20] Q. Meng, K. Geng, and J. Lu, "Experimental investigation on friction and wear characteristics of laser-clad Stellite 6 coating under dry sliding conditions" Tribology International, vol.145, 106298, 2020, https://doi.org/10.1016/j.triboint.2020.106298

[21] Z. Liu, and Y. Li, "Influence of Cr content on corrosion resistance of laser-clad Co–Cr–W coatings" Journal of Alloys and Compounds, vol.504, no.2, pp.345-350, 2010, https://doi.org/10.1016/j.jallcom.2010.05.124

[22] M. Y. Yin, et al. "Study on electrochemical corrosion behavior of Y2O3-doped AlCrFeNiTi high-entropy alloy laser cladding coatings." Journal of Materials Research and Technology, vol42, pp.2940-2953, 2026, https://doi.org/10.1016/J.JMRT.2026.03.234

[23] Z. H. Yuan, et al. "Fretting Wear and Corrosion Behavior Study of CrAlN and CrAlSiN Coatings in Lead-Bismuth Environment (LBE)." High Temperature Corrosion of Materials, vol.103, no.2, pp.30-30, 2026, https://doi.org/10.1007/S11085-026-10387-1

[24] M. J. Yan, et al." Microstructure and corrosive wear behavior of Fe-based amorphous coatings prepared by extreme high-speed laser cladding." Journal of Materials Research and Technology, vol.39, pp.4882-4897, 2025 https://doi.org/10.1016/J.JMRT.2025.10.185

https://doi.org/10.64486/m.65.4.14